Inversion Breakup in Small Rocky Mountain and Alpine Basins

C. DAVID WHITEMAN,* BERNHARD POSPICHAL,+ STEFAN EISENBACH,+ PHILIPP WEIHS,#
CRAIG B. CLEMENTS,@ REINHOLD STEINACKER,+ ERICH MURSCH-RADLGRUBER,#
AND MANFRED DORNINGER+

*Pacific Northwest National Laboratory, Richland, Washington
+Department of Meteorology and Geophysics, University of Vienna, Vienna, Austria
#Institute for Meteorology and Physics, University of Natural Resources and Applied Life Sciences, Vienna, Austria
@Department of Earth and Ocean Sciences, University of British Columbia, Vancouver, British Columbia, Canada

(Manuscript received 14 August 2003, in final form 1 March 2004)

ABSTRACT

Comparisons are made between the postsunrise breakup of temperature inversions in two similar closed basins in very different climate settings, one in the eastern Alps and one in the Rocky Mountains. The small, high-altitude, limestone sinkholes have both experienced extreme temperature minima below −50°C and both develop strong nighttime inversions. On undisturbed clear nights, temperature inversions reach to 120-m heights in both sinkholes but are much stronger in the drier Rocky Mountain basin (24 vs 13 K). Inversion destruction takes place 2.6–3 h after sunrise in these basins and is accomplished primarily by subsidence warming associated with the removal of air from the base of the inversion by the upslope flows that develop over heated sidewalls. A conceptual model of this destruction is presented, emphasizing the asymmetry of the boundary layer development around the basin and the effects of solar shading by the surrounding ridgeline. Differences in inversion strengths and postsunrise heating rates between the two basins are caused by differences in the surface energy budget, with drier soil and a higher sensible heat flux in the Rocky Mountain sinkhole. Inversions in the small basins break up more quickly following sunrise than for previously studied valleys. The pattern of inversion breakup in the non-snow-covered basins is the same as that reported in snow-covered Colorado valleys. The similar breakup patterns in valleys and basins suggest that along-valley wind systems play no role in the breakups, since the small basins have no along-valley wind system.

1. Introduction

Strong temperature inversions can form in mountainous terrain in clear undisturbed weather, leading to serious air pollution problems, persistent fog and stratus, and disruptions to ground and air transportation. The trapping of cold air within the inversions affects agricultural production and leads to extreme temperature minima. The breakup of valley and basin inversions is a particularly difficult weather forecasting problem. For this reason, an expert panel (Smith et al. 1997) has called for enhanced research on the mechanisms that lead to the breakup of valley and basin inversions. Recent observational studies in valleys and large basins have approached the problem from an energetics framework, studying the effects on inversion breakup of heat transfer to the valley or basin atmosphere. These studies have been hampered by difficulties in measuring the influence of along-valley advection on heat transfer, since total advection is the small difference between two large terms that are difficult to measure, vertical advection and horizontal advection.

Because the confounding effects of advection by along-valley winds are eliminated in small enclosed basins and because their small size makes such basins easier to instrument, two studies of the temperature inversion life cycle were recently conducted in small basins of similar size in the Rocky Mountains (Clements et al. 2003) and the Austrian Alps (Steinacker et al. 2002; Whiteman et al. 2004a,b). Data from these experiments are used in this paper. A detailed description of the Peter Sink experiments was published by Clements et al. (2003), and a comprehensive overview of the Gruenloch experiments is being submitted for publication (R. Steinacker 2004, personal communication) so that the experiments are only briefly described in this paper. The two basins are small, remote, high-elevation, limestone sinkholes that are known for producing extreme temperature minima. The Gruenloch (or Gstettneralm) sinkhole or *doline* in the eastern Alps near Lunz, Lower Austria, has recorded an extreme minimum temperature of −52.6°C. The Peter Sink, on the crest of Utah's Bear River Range, has reached temperatures as low as −56.3°C (Pope and Brough 1996). The remote

Corresponding author address: C. David Whiteman, Pacific Northwest National Laboratory, P.O. Box 999, Richland, WA 99352.
E-mail: dave.whiteman@pnl.gov

location of these sinkholes did not allow experiments to investigate the extreme minimum temperature events that occur in winter, but the extreme cooling in the sinkholes is also seen in other seasons and the experiments were focused on investigating the physical processes that lead to strong cooling in the sinkholes and the associated strong temperature inversions. In both basins, series of tethered balloon soundings were made during the postsunrise temperature inversion breakup period. The purpose of this article is to use these data to investigate inversion breakup in the two sinkholes, reporting on the similarities and differences of the wind and temperature structure evolution in the two sinkholes, comparing the inversion breakups in these small enclosed basins with inversion breakups in valleys and, to the extent that data allow, investigating the surface energy budgets and atmospheric energetics during the inversion breakup periods.

A number of previous studies have investigated the buildup and breakup of temperature inversions in basins. The *buildup* of temperature inversions in basins has received research attention that was summarized by Geiger (1965). The impetus for the studies reported by Geiger was to determine the causes of extreme temperature minima and their impacts on human habitats, especially in agricultural areas. More recent investigations of inversion buildup (e.g., Magono et al. 1982; Yoshino 1984; Maki and Harimaya 1988) have extended to studies of basin heat budgets during nighttime (Maki et al. 1986; Kondo et al. 1989; Whiteman et al. 1996), the role of downslope flows on inversion development (Mori and Kobayashi 1996), and the seasonal variation of radiation on inversion characteristics (Iijima and Shinoda 2000). To date, inversion *breakup* has been investigated primarily on cross sections of relative large valleys (e.g., Whiteman 1982; Whiteman and McKee 1982; Müller and Whiteman 1988; Bader and McKee 1983, 1985; Sakiyama 1990), in large basins (Banta and Cotton 1981; Banta 1984; Whiteman et al. 1999a, 2001; Zhong et al. 2001), but also in a relatively small 84 km^2 Colorado basin (Whiteman et al. 1996; Fast et al. 1996). To our knowledge, no previous studies of inversion breakup have been conducted in basins of the small size (approximately 2 km^2) of the Peter Sink and Gruenloch basins.

The Gruenloch basin, because of its longstanding reputation for extreme temperature minima (Geiger 1965) and its proximity to the Lunz Biological Station (Bretschko and Adamicka 1998), has been the site of previous biological and meteorological (e.g., Sauberer and Dirmhirn 1954, 1956; Litschauer 1962) research. The meteorological research, as for other basins, has focused primarily on temperature minima and nighttime temperature inversions. Sauberer and Dirmhirn, however, included two temperature soundings in their 1954 paper that were made partway through the postsunrise temperature inversion breakup period. These soundings, conducted on an early March morning with snow cover, showed warming progressed downward into the basin from aloft during the inversion destruction period. As we will see, our data collected during a non-snow-covered case in early June show similar characteristics. Other characteristics of inversion breakup in these sinkholes provided interesting surprises. The inversion breakup times were shorter in these basins than in valleys that have been studied previously; despite substantial differences in inversion strengths in the two basins the time required to break the inversions was nearly identical; the inversion breakup pattern in the small enclosed basins was very similar to that seen in *snow-covered valleys* in Colorado; and these similar valley/basin breakup patterns occurred despite the absence of along-valley wind systems in the basins.

2. Basin topography

Topographic maps of the two basins are shown in Fig. 1. The Gruenloch, on the Hetzkogel Plateau 5 km south of Lunz, Austria, has a floor elevation of 1270 m MSL and is completely surrounded by higher terrain up to the lowest pass (the Lechner Saddle) northwest of the basin center at 54 m above the basin floor (ABF). The Peter Sink, located in the United States on the crest of Utah's Bear River Range 150 km NNE of Salt Lake City, has a floor elevation of 2500 m MSL and its lowest pass is to the southwest of the basin at an elevation of 35 m ABF. This pass connects the sinkhole to another sinkhole lobe.

Figure 2 shows the heights above the basin floor of the ridgelines surrounding the basins. The Peter Sink is seen to have relatively low ridgelines, with no topography exceeding 153 m ABF. Relatively low saddles or passes are found at elevations of 35–75 m ABF to the NNW, NNE, E (East Saddle), and SSW (South Gap) of the basin center. The Gruenloch, in contrast, is surrounded by more variable terrain, including a major peak, the Hühnerkogel (1651 m MSL). The passes are fewer and at higher elevations than for the Peter Sink. Major passes are found to the SW (Ybbstaler Saddle), NW (Lechner Saddle), and ESE (Seekopfalm Saddle) of the basin center. The Lechner Saddle is the only pass whose elevation is below 120 m ABF, the depth of typical nocturnal inversions.

Figure 3 shows the drainage areas and atmospheric volumes for the two basins as determined from detailed topographic maps using a planimeter. The computations for each basin were made up to the highest points on the ridgelines (i.e., the elevations at the left-hand sides of Figs. 2a,b), assuming vertical boundaries above the lower ridgeline terrain (dashed lines in Fig. 1 and upper boundary of shaded areas in Figs. 2a,b). Cumulative basin volume as a function of height was obtained by summing the volumes of atmospheric layers between adjacent terrain contours calculated as the volume of the frustrum of a cone. The basins have comparable total drainage areas (2.25 km^2 for the Peter Sink and 1.82

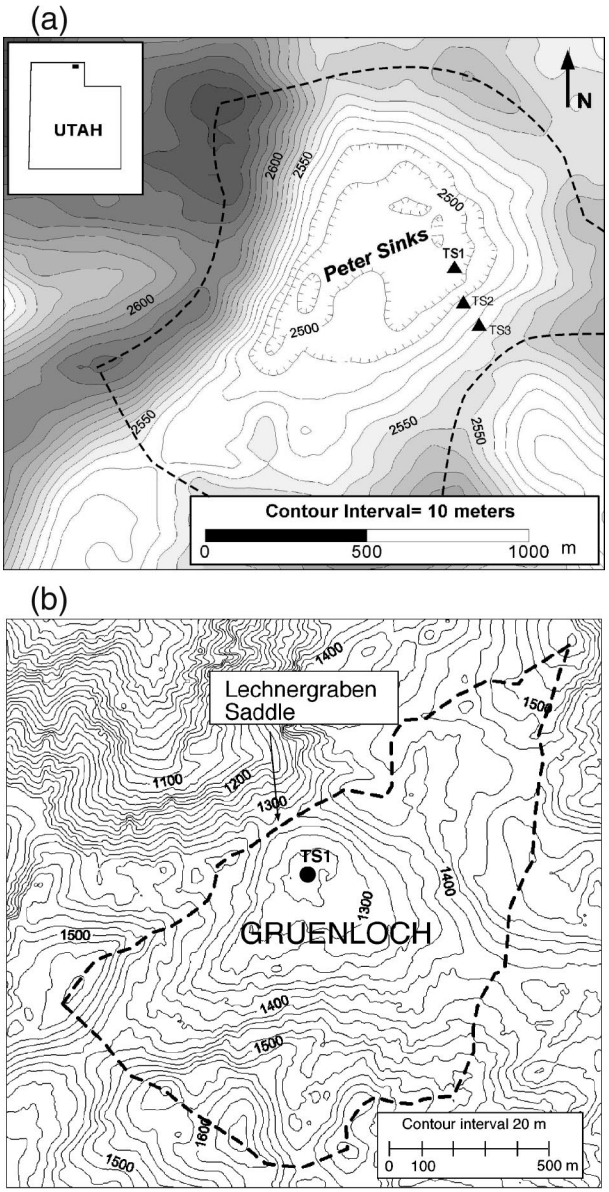

FIG. 1. Topographic maps of the (a) Peter Sink and (b) Gruenloch basins showing the tethersonde locations (TS1–TS3) and the basin boundaries (dashed lines).

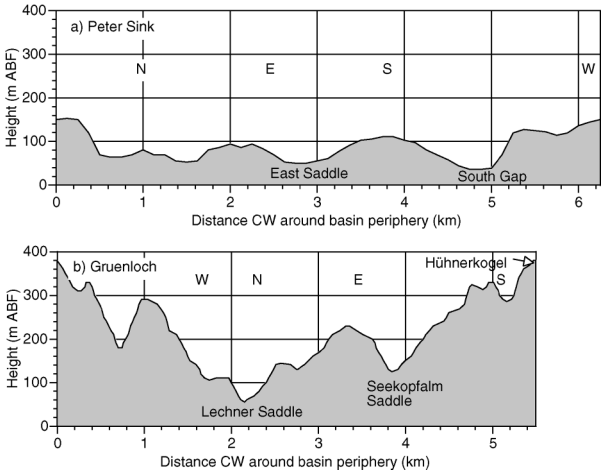

FIG. 2. Ridgeline elevations as a function of clockwise distance around the basins for (a) the Peter Sink and (b) the Gruenloch basins. The ridgelines are shown as dashed lines in Fig. 1. Major gaps or saddles in the ridgeline are indicated, as are the cardinal directions.

km^2 for the Gruenloch), but the Gruenloch atmospheric volume is 174% of the Peter Sink's volume.

The slope angles are somewhat variable around the Peter Sink basin. The east slope has an angle of about 11°, the north slope 13°, and the west slope 28°. The annual precipitation in the sinkhole is an estimated 1040 mm (T. Wright 2003, personal communication). Vegetation in the basin is rather sparse, as it is in a dry climate that is also grazed in the summer by cattle and sheep. Vegetation type depends primarily on slope aspect. The east slope contains mostly short grasses (<0.5 m) and sagebrush (~0.75 m). The north slope supports a sparse distribution of sagebrush and small shrubs (<0.5 m). The basin floor has short grasses (<0.1 m) and bare soil. Conifers are found on the basin crest. The lower half of the west slope contains talus; short conifers grow on the upper two-thirds of this slope. Soil type depends on location, but generally consists of loose clay and sandy alluvium. Observations were made following an unusually dry summer and the soil was very dry, with much dust on the roads and trails.

The Gruenloch is a near-circular sinkhole with uniform slope angles of about 15°–20°. The slopes to the northeast are slightly steeper than those to the southwest.

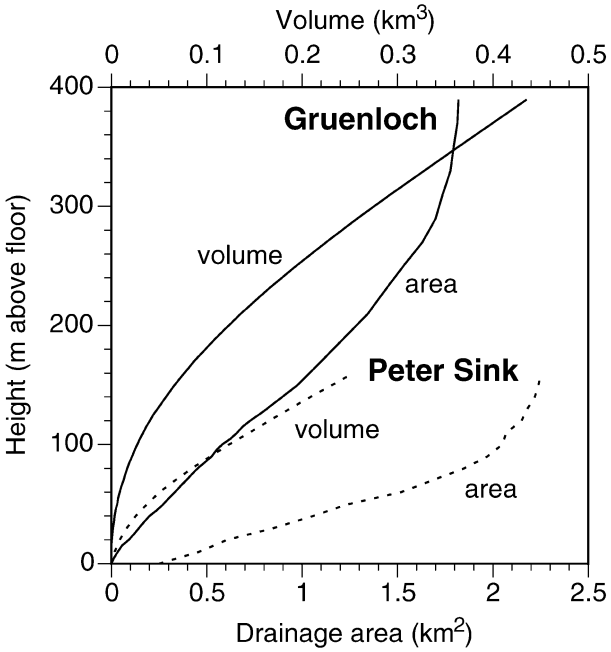

FIG. 3. Drainage areas (km^2) and volumes (km^3) as a function of height for the two basins.

The basin floor is 60–100 m in diameter, and there is a small pond (less than 10 m in diameter) that contains water all year long at the lowest elevation. The sinkhole is situated on a limestone plateau in one of the wettest parts of the Eastern Alps, with an annual precipitation of 2200 mm. The limestone bedrock of the sinkhole is covered by a deep humus layer on the basin floor, but the slopes have only a thin layer of soil (decreasing with altitude), with bare rock exposed at some locations. Rather unusually for this part of the Alps, the distribution of vegetation does not depend on slope aspect. In spite of the humid soil, tall conifers grow only on the higher-elevation slopes and on the ridge crests. The lower slopes have sparse dwarf pine trees, similar to what is found at other locations at much higher altitudes. Last, the basin floor has only grasses and other subalpine herbaceous plants, as the low minimum temperatures hinder the growth of trees. Only plants that are covered by a well-insulating snow cover can survive such hostile conditions. Thus, both the Gruenloch and Peter Sink exhibit a distinct ''vegetation inversion,'' with no trees at the lowest elevations of the basins.

3. Observations

a. Tethered balloon soundings

Tethered balloon soundings were made from the floors of the Peter Sink and Gruenloch basins during the clear, undisturbed mornings of 9 and 12 September 1999 and 3 and 4 June 2002, respectively. Astronomical sunrise on these dates was 0604 and 0607 mountain standard time (MST) and 0410 and 0409 central European standard time (CEST), respectively. Local sunrise times at different locations within the basins were variable depending on shadows cast by the surrounding ridgelines. Shadows were particularly prevalent in the lower altitudes of the Gruenloch because of the relatively high ridgeline to the northeast and east of the basin center.

Tethered balloon soundings from the 9 September (Peter Sink) and 3 June (Gruenloch) tethered balloon experiments (Fig. 4) are chosen for comparison, as the soundings on these dates followed clear, undisturbed nights when typical inversions were thought to have developed in the basins. The inversions in both basins extended to about 120 m ABF, but the Peter Sink inversion was much stronger (24 vs 13 K).

In the Peter Sink basin (Fig. 4a), the 0505 and 0607 MST pre- and near-sunrise soundings found a two-layer atmosphere in the basin. A 70-m-deep layer with a potential temperature increase of 4.5 K was surmounted by a 50-m-deep layer containing a potential temperature jump of 19.5 K! The development of this structure during the previous night was described by Clements et al. (2003). The inversion was destroyed after sunrise by a warming in the basin produced by subsidence and, especially later in the breakup period, by the upward growth of a convective boundary layer (CBL) from the heated basin floor. The compensatory subsidence over the center of the basin occurs in response to the removal of air from the basin inversion by upslope flows that develop over the heated sidewalls. These sinking motions effectively transfer the heat released at the sidewalls through the entire basin cross section. This type of inversion destruction, in which the inversion is destroyed by a combination of subsidence and CBL growth has been termed a pattern-3 inversion destruction (Whiteman 1982). The inversion was destroyed between the 0829 and 0854 MST soundings, approximately 2.6 h after astronomical sunrise. Mixing ratios above the basin were only about 2 g kg^{-1}. The mixing ratios were slightly higher inside the basin, but decreased again in the lowest tens of meters above the basin floor. During the inversion breakup period the mixing ratios increased near the basin floor and were mixed upward, moistening the atmosphere through and above the basin by 0926 MST. Winds were calm inside the basin inversion at sunrise, but increased to 4 m s^{-1} above the top of the basin inversion. The winds above the inversion decreased after sunrise to 1–1.5 m s^{-1}, but the winds increased in the basin to 1–3 m s^{-1} as the inversion destruction progressed. These east-through-south winds are cross-basin flows that blew toward the most strongly heated sidewalls.

Tethered balloon soundings in the Peter Sink were made concurrently from three sites (Fig. 1) on the floor and east sidewall of the sinkhole. Comparisons between the soundings made at specific times during the inversion breakup period (Fig. 5) show that potential temperature exhibited little horizontal variation between sites in the bulk of the inversion, except in the near-ground layers at each site where nocturnal boundary layers, present initially, were eventually replaced by convective boundary layers after sunlight illuminated the underlying slopes.

In the Gruenloch basin (Fig. 4b), the first up-sounding near sunrise did not go high enough to determine the inversion depth. The 0514 sounding, however, showed that the potential temperature increased linearly from the surface to 120 m with a temperature increase of 13 K. The near-sunrise soundings show a temperature jump at the altitude corresponding to the Lechner Saddle. Nighttime temperatures are comparatively colder in the enclosed cold-air pool below this outlet height. The strong stability at the top of this pool effectively isolates the lower pool from the partially enclosed atmosphere above, where nighttime drainage flows exit through the Lechner Saddle. The basin floor was in shadow during most of the inversion breakup period, so that no CBL was noted at the base of any of the soundings. Soundings ended before the inversion was completely destroyed, but we estimate from surface temperature records on the basin floor that the inversion was destroyed at about 0710 CEST, about 3 h after sunrise. Destruction was caused by subsidence warming of the basin atmosphere

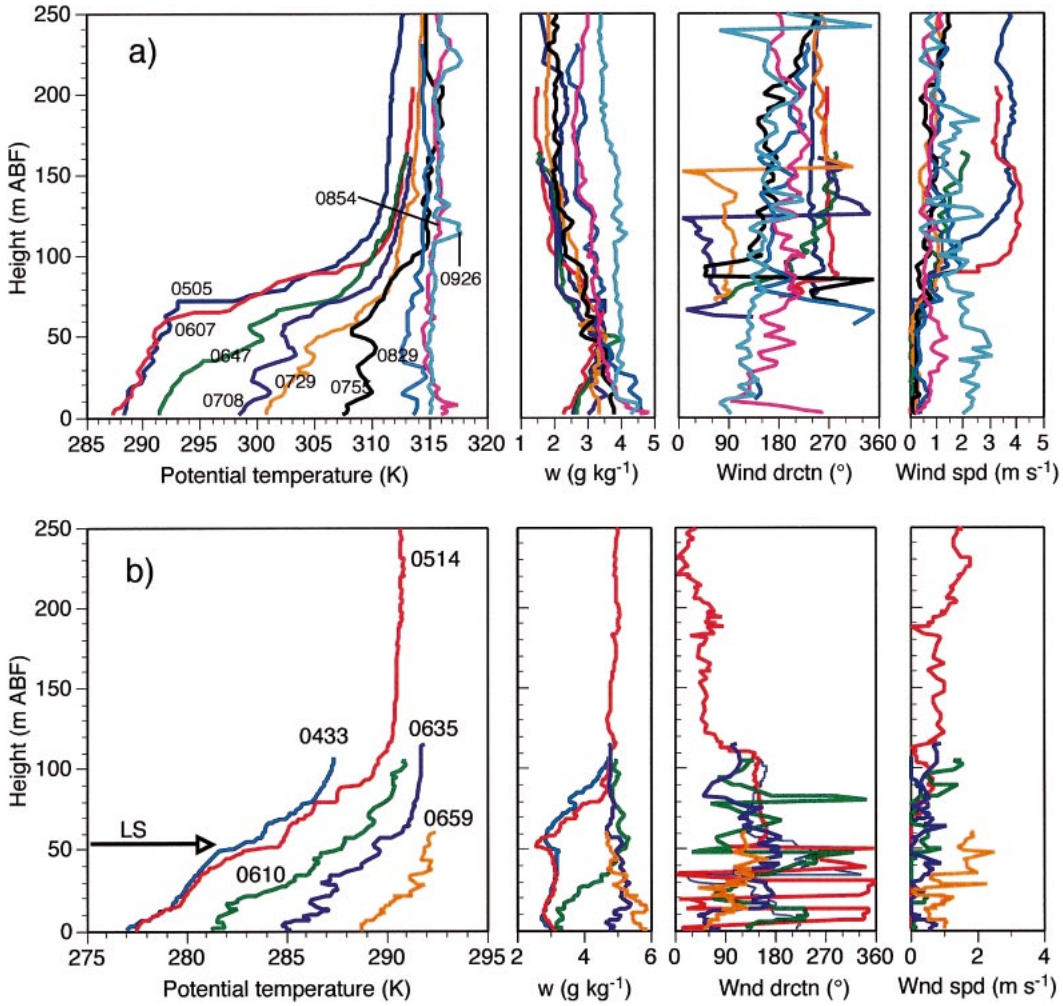

FIG. 4. Tethered-balloon up soundings in (a) the Peter Sink 9 Sep 1999 and (b) the Gruenloch 3 Jun 2002. Peter Sink times are MST; Gruenloch times are CEST. The arrow labeled LS indicates the height of the Lechner Saddle. For legibility, wind directions were not plotted in (a) for heights at which speeds were 0.4 m s^{-1} or less.

where the subsidence compensated for the removal of air from the inversion by upslope flows on the heated sidewalls. This type of inversion destruction has been termed a pattern-2 destruction (Whiteman 1982). The air within the enclosed lower basin (below the Lechner Saddle) at sunrise was drier than the air above the basin (mixing ratios w of 3 vs 5 g kg^{-1}) with a gradual increase in mixing ratio above the level of the saddle. The moisture deficit inside the lower enclosed basin (i.e., below the Lechner Saddle) was produced by condensation and sublimation of moisture onto the basin floor and sidewalls. A remoistening of the basin atmosphere occurred during the inversion breakup period as air with a higher moisture content was brought downward into the lower basin from aloft and as evaporation occurred at the ground. At sunrise, the winds within the inversion were calm below the height of the Lechner Saddle. Above this height (but still within the inversion) weak southeast winds (<0.5 m s^{-1}) blew through the Lechner Saddle. As the inversion breakup proceeded, winds both below and above the Lechner Saddle blew from the northeast through south toward the most strongly heated sidewalls, with wind speeds increasing to 2 m s^{-1} near the end of the inversion destruction period. This cross-basin flow toward the most strongly heated sidewall, seen in both the Gruenloch and Peter Sink observations, has been noted in valleys, where it is termed a cross-valley flow.

It took about the same amount of time after sunrise (2.6–3 h) to break the two basin inversions, despite the much stronger inversion in the drier climate setting of the Peter Sink. The drier setting produces more outgoing radiation at night, stronger inversions at sunrise, but also stronger heating after sunrise and, thus, similar destruction times. The effect of the climate in producing inversions of different strength is supported by calculations of the heat losses accumulated in the basins from the last well-mixed sounding of the afternoon until sun-

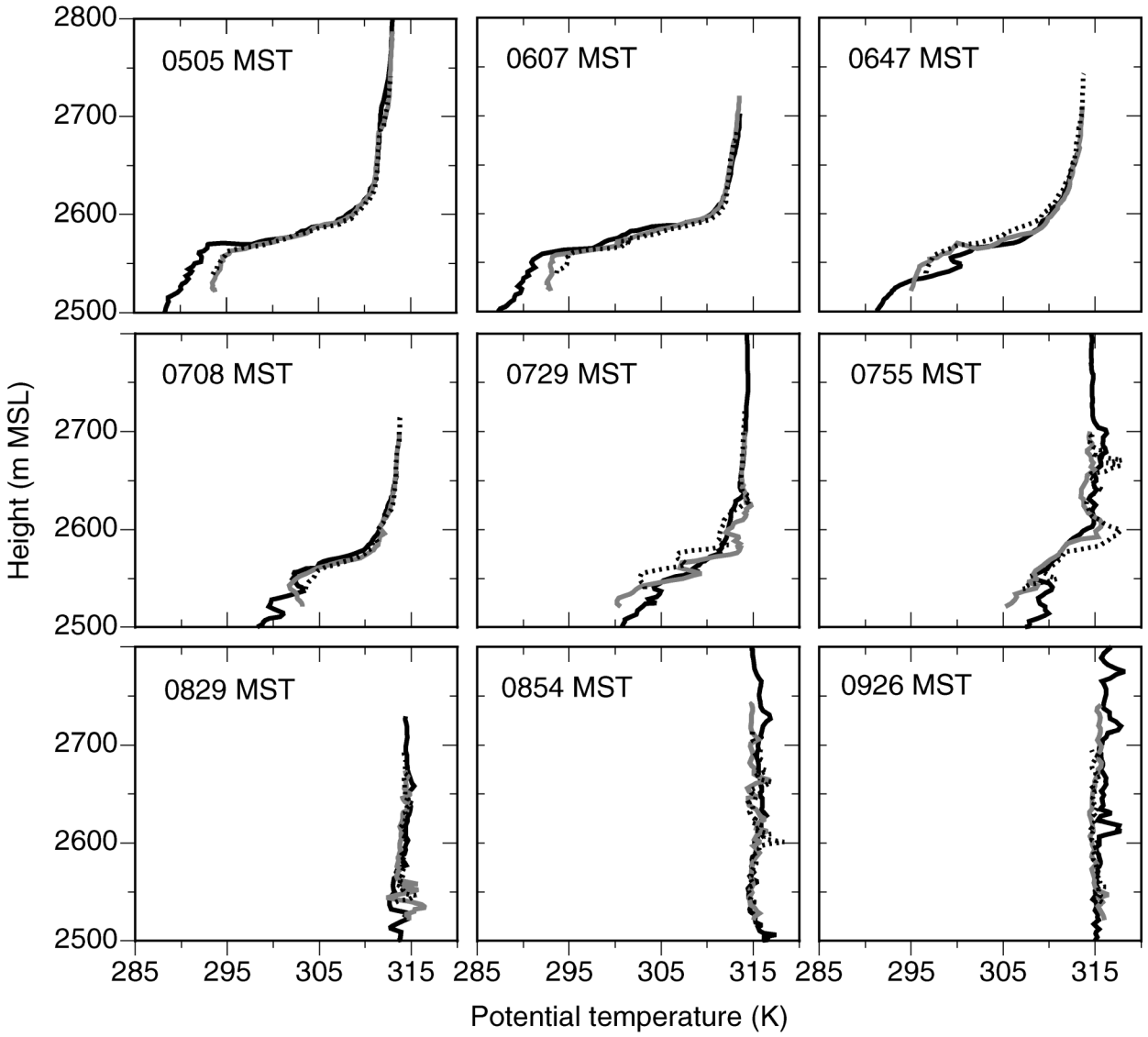

FIG. 5. Concurrent soundings of potential temperature from the floor and east sidewall of the Peter Sink at various times during the inversion breakup period of 9 Sep 1999. The locations of the soundings at TS1 (black line), TS2 (gray line), and TS3 (dashed line) were shown in Fig. 1a. The TS1 site was on the basin floor (2500 m MSL), while the TS2 and TS3 sites were at different heights (2521 and 2539 m MSL, respectively) on the east sidewall of the basin.

rise (not shown). The Peter Sink heat loss on 8–9 September was 1.00 MJ m^{-2} while the Gruenloch heat loss on 2–3 June was 0.39 MJ m^{-2} (here, the Gruenloch heat loss was accumulated to a height of only 105 m rather than 120 m because the tethersonde data often did not extend to the 120-m height), showing that the heat losses, like the heat gains, are greater in the Peter Sink than in the Gruenloch. The inversion breakup times in the two sinkholes are shorter than the 3.5–5 h required for destruction of deeper inversions in wider Colorado (Whiteman 1982; Whiteman and McKee 1982) and Swiss (Müller and Whiteman 1988) valleys, and the approximately 9 h required in a large Japanese basin (Kondo et al. 1989). The shorter breakup times in smaller basins indicates an enhanced effectiveness of heat transfer in the smaller volume from convection, conduction, and radiation.

The extreme minimum temperatures reported for the Peter Sink and Gruenloch differ by only a few degrees Celsius (−56.3° vs −52.6°C) while the inversion strengths in the two basins are substantially different (24 vs 13 K). If these relative inversion strengths are representative of the meteorological conditions (fresh snow cover, clear skies, and the advection of extremely cold air above the sinkholes) that produce the temperature extremes, we might surmise that the temperatures above the Gruenloch fall to lower values than those above the Peter Sink. This cannot be tested, however,

as vertical soundings are unavailable for the temperature extreme cases. Long-term measurements are available for a longer period of time in the Gruenloch, so that the −56.3°C minimum in the Peter Sink may not be truly representative of the extremes that can be attained there in climatologically unusual events.

b. Surface energy budget measurements

Radiation and surface energy budget measurements from the two basins for 12 September and 3 June are shown in Figs. 6a and 6b. The data in the 3 h after astronomical sunrise are of most interest for the present study. Extraterrestrial solar radiation curves in these figures are values obtained for a horizontal surface from a theoretical solar model (Whiteman and Allwine 1986) that accounts for the day of year, time of day, and latitude and longitude, but does not account for atmospheric attenuation. Actual incoming solar radiation was not measured in these experiments but a first estimate of this, in accordance with measurements made by Whiteman et al. (1989a) in a September experiment in a high-altitude setting in the Rocky Mountains similar to the Peter Sink, is that the incoming solar radiation would be about 0.71 of the extraterrestrial curve when in direct sunlight. A curve made under this assumption is included as a dashed line in Fig. 6a. Measured values of net radiation at the floor of the Peter Sink and at two sites in the Gruenloch and sensible heat flux at the floor of the Peter Sink are also shown. The delay of local sunrise relative to astronomical sunrise in both basins is apparent in the figures, with a 1-h delay on the floor of the Peter Sink, a 2-h delay on the floor of the Gruenloch, and a delay of more than 5 h at a site on the east sidewall of the Gruenloch. Shadows cast from surrounding trees and the effects of late afternoon cloudiness are apparent in the Gruenloch curves. The measured net radiation levels (Fig. 6) are in accordance with other measurements performed in mountainous areas (Marty and Philipona 2001; Sauberer and Dirmhirn 1958). Despite the lower altitude of the Gruenloch compared to the Peter Sink, which might be expected to increase atmospheric attenuation of the solar beam, we observed higher net radiation levels in the Gruenloch. The explanation lies primarily in the smaller solar zenith angle at the same local time at Gruenloch in June than at Peter Sink in September. In addition and among other factors such as atmospheric turbidity, albedo, and ground temperature, the partial cumulus cloudiness at Gruenloch on that day may have enhanced the net radiation. On the one hand, reflections at the cloud edges toward the observer may result in enhancements in maximum downward shortwave radiation levels compared with clear-sky conditions (Segal and Davis 1992). On the other hand, an enhancement in longwave radiation compared to clear-sky levels of around 80 W m^{-2} (Sauberer and Dirmhirn 1958) may occur because of the higher

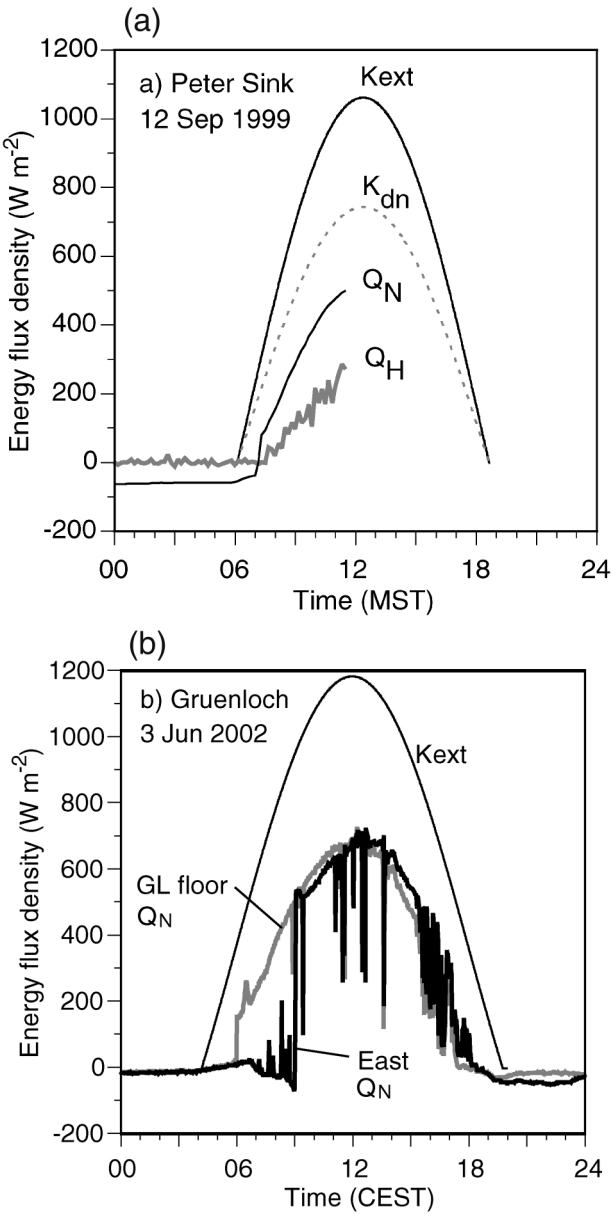

FIG. 6. Radiative and surface heat fluxes on the floor of (a) the Peter Sink 12 Sep 1999 and (b) the Gruenloch 3 Jun 2002. Shown are theoretical values of extraterrestrial solar flux (K_{ext}) and measured values of net all-wave radiation (Q_N) and sensible heat flux (Q_H). Also shown in (a) is an estimate of the downward solar radiation ($K_{dn} \sim 0.71K_{ext}$). The two Q_N curves in (b) are from instruments on the floor of the Gruenloch and on the east sidewall 30 m above the floor.

temperature of the cumulus clouds when compared with the background atmosphere at higher altitudes.

A negative peak of net radiation occurs at the east sidewall just before the rapid increase in radiation at 0900 CEST. The explanation lies in a sudden increase in upward ground-reflected radiation as the sunlit areas in the surroundings move closer to the pyrradiometer. An increase in reflected shortwave radiation therefore

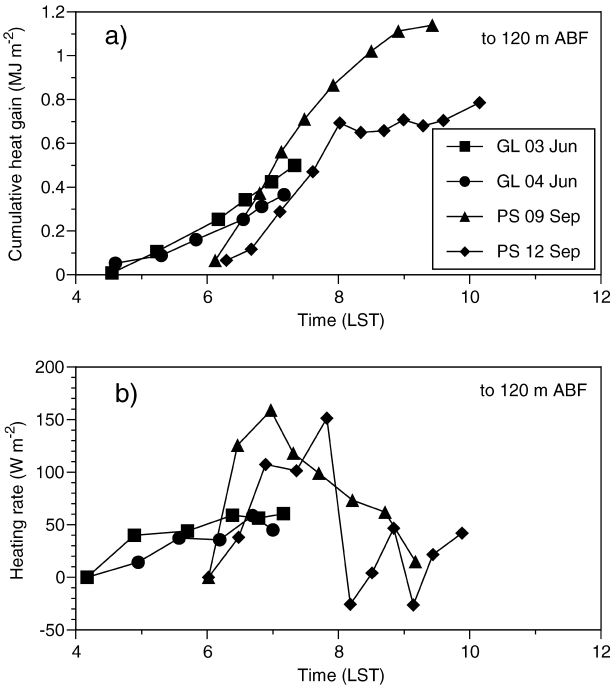

FIG. 7. (a) Cumulative heat gain (MJ m^{-2}), and (b) the rate of heat gain (W m^{-2}) as integrated up to 120 m ABF in the Gruenloch (GL) and Peter Sink (PS) basins for the dates indicated (Gruenloch dates in 2002; Peter Sink dates in 1999). Times are local standard time (LST).

occurs before the pyrradiometer emerges from the shade.

4. Analysis of inversion breakup energetics

Computations of the fluxes of heat into and out of the basin atmospheres during the inversion destruction period are shown in Fig. 7. Figure 7a shows the cumulative heat gains to the basin atmospheres following sunrise as accumulated with time and to a height of 120 m ABF using the formula

$$S = \frac{\int_0^{h=120\ \mathrm{m}} c_p \rho(z)[\theta(z) - \theta_1(z)]A(z)\, dz}{A_h} \ (\mathrm{J\ m^{-2}}), \quad (1)$$

where $\theta_1(z)$ is the potential temperature sounding just before sunrise and $\theta(z)$ is the postsunrise vertical potential temperature sounding of interest, c_p is the specific heat of air at constant pressure, $\rho(z)$ is the air density, $A(z)$ is the basin drainage area, and potential temperature is assumed to be horizontally homogeneous within the basin. The value S has been calculated for sequences of tethered balloon ascents, and the 120-m integration height has been chosen to correspond to the nocturnal inversion heights on 3 June (Gruenloch) and 9 September (Peter Sink). Inversion heights on 4 June and 12 September were 95 and 130 m ABF, respectively. The division by A_h in Eq. (1) facilitates comparisons between basins of different size. For the Peter Sink, A_h was 2.15 km^2; for the Gruenloch, A_h was 0.73 km^2 (Fig. 3).

The rates of heat gain, as determined from the slope of the cumulative heat gain curve in Fig. 6a between consecutive pairs of potential temperature profiles, are shown in Fig. 7b. The rate in the Peter Sink rises rapidly after sunrise, reaching 160 W m^{-2} within 2 h after sunrise. The rates then drop as the inversion is destroyed and the input of sensible heat becomes distributed through a much deeper convective boundary layer extending above the basin (and above the 120-m-deep calculation volume).

5. Discussion

This section will extend consideration of several topics that arise from the analyses, including 1) the evolving three-dimensional structure of the basin atmosphere during the inversion breakup period, 2) basin heat deficits, 3) the relationship between atmospheric and surface heat budgets in different climate settings, and 4) a comparison of inversion breakup processes in basins and valleys.

a. Three-dimensional inversion breakup structure

A conceptual model of inversion breakup in closed basins during clear, undisturbed conditions is given in Fig. 8, as modified from conceptual models of valley inversion breakup by Whiteman (1982) and Brehm (1986). At sunrise, the nocturnal inversion that built up during the night extends across the basin from sidewall to sidewall. Isentropes or isotherms are nearly horizontal in this inversion (Whiteman et al. 2004a), except in a shallow layer of several meters depth adjacent to the slopes where the isentropes tilt upward, indicating the temperature deficit that drives the nighttime downslope flows. Following sunrise, the basin sidewalls are heated by insolation. The insolation received depends on a slope's exposure to the sun's rays, which depends on the inclination angle of the slope, its azimuth angle, the position of shadows cast by surrounding terrain, and the sun's position in the sky at a given date and hour. In basins, insolation varies continuously around the basin circumference, while in a simple linear valley the insolation is received on two sidewalls having azimuth angles that differ by 180°. For simple basin topography, the sunlight–shadow interface progresses down the east-facing sidewall. The sunlight heats the ground and, through the surface energy budget, produces an upward sensible heat flux that develops a convective boundary layer above the heated valley surfaces. Convection removes mass from the overlying remnant of the nocturnal inversion and this mass is carried upslope by upslope flows that form in the shallow heated convective boundary layer. As compensation for the upslope flows over the sidewalls, weak subsidence occurs over the basin.

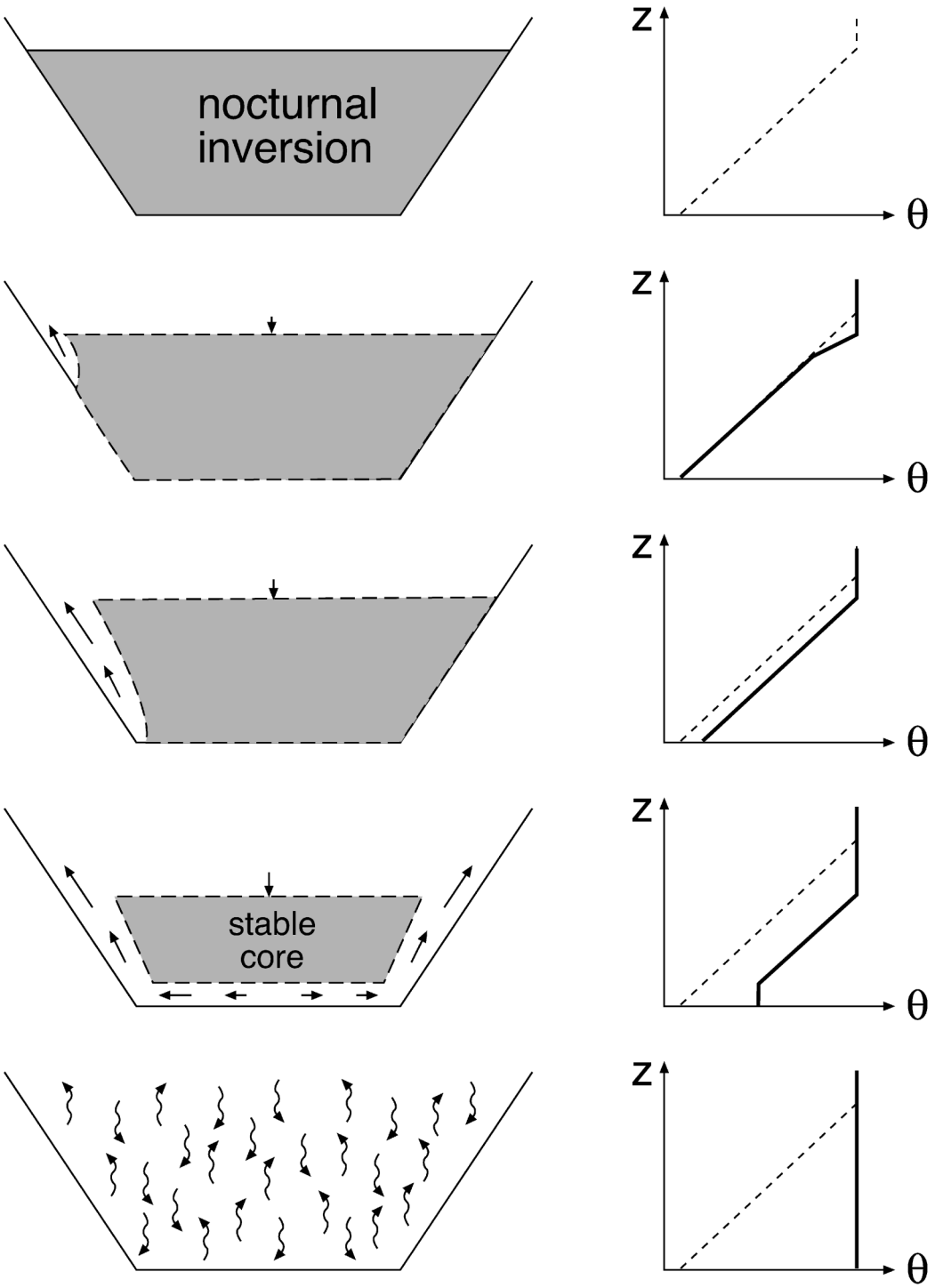

FIG. 8. Schematic diagram of (left) successive cross sections and (right) corresponding potential temperature soundings in a closed basin during successive times (top) starting just before sunrise and (bottom) ending when the inversion is broken. The dashed line, repeated in all potential temperature plots, shows the presunrise sounding. The cross sections show sunlight progressing down the left sidewall of the basin until both sidewalls eventually become illuminated.

The sinking rate is stronger in narrower (as opposed to wider) basins and in basins that develop stronger upslope flows (e.g., in climate settings where available energy at the surface is partitioned mainly into sensible heat flux). The subsidence rate varies with height, as the mass budget requires that air mass carried up the sidewalls in the shallow upslope flows be balanced by sinking motions over the broader basin at the same height, and both the mass carried by the upslope flows and the basin horizontal area vary with elevation. The subsidence is probably not uniform over the entire horizontal area of the basin at a given height; the tendency for the isentropes to remain horizontal under the influence of gravity (see Fig. 5 and simulations by Colette et al. 2003) causes mass to be moved in cross-basin flows toward locations where upslope flows remove mass from the edges of the inversion. The compensatory sinking motions produce advective warming ($\partial\theta/\partial t = -w\partial\theta/\partial z > 0$) in the uppermost layer of the inversion. The sinking motions and associated warming progress deeper into the basin as the sunlight progresses down the sidewall. Once the basin floor and other sidewalls are illuminated, a continuous convective boundary layer may be present over the topography or parts of the topography, and inversion destruction progresses through continued sinking/warming of the bulk of the stable core or through the upward growth of the convective boundary layer from the underlying heated slopes or basin floor. The relative rates of growth of the CBL and sinking of the stable core depend on the basin width (wider basins favor CBL growth) and the rate of release of sensible heat (higher rates of sensible heat flux favor CBL growth). Complete inversion destruction occurs when the entire basin attains the potential temperature of the air above the stable core, so that no elevated remnants of the nocturnal inversion remain. It should be kept in mind that the ''snapshots'' in Fig. 8 are not equally spaced in time. The progression of the inversion destruction and whether CBL growth is seen in the basin floor soundings depends on shadows cast by the topography and other factors that are variable from basin to basin (Colette et al. 2003).

The Peter Sink and Gruenloch basins are in climate settings where the surface energy budgets are quite different. The dry climate of the Peter Sink produces relatively high rates of release of sensible heat compared to those in the moist climate setting of the Gruenloch. These differing rates of heat release are responsible for the differing patterns of inversion breakup in the two basins, pattern 3 (CBL growth and subsidence) in the Peter Sink and pattern 2 (primarily subsidence) in the Gruenloch. Both basins have well-developed inversions at sunrise. Observations in both sinkholes (Clements et al. 2003; Whiteman et al. 2004a) show that the isentropes are near horizontal in the nocturnal inversion. After sunrise, distinctive S-shaped potential temperature sublayers are often seen in the potential temperature profiles (see Figs. 4a,b, especially the 0647, 0708, 0729, and 0755 MST soundings in the Peter Sink and the 0635 CEST sounding in the Gruenloch). These sublayers, which occur before the basin floors are well illuminated but while sunlight is strongly heating the east-facing slopes, appear to be produced by horizontal eddies within the stable core or by gravity waves (Bader and McKee 1983) that are excited by convection impinging on the inversion margin above the heated sidewall. The cross-valley flow toward the heated sidewall has been previously noted in valleys that have strong differences in insolation on the opposing sidewalls (Urfer-Henneberger 1970; Hennemuth 1986). Other studies have deduced this flow from measurements of tracer plume deposition on the heated sidewall (Whiteman 1989) and through numerical model simulations (Bader and Whiteman 1989). Late in the inversion breakup period in the Peter Sink, similar S-shaped deformations occur in the CBL that grows upward from the heated basin floor and from the sidewalls (Fig. 5). These deformations appear to be convective plumes rising from the underlying heated surface.

In the Peter Sink and Gruenloch basins, the air above the inversion top continues to warm during the inversion destruction period, a feature that varies from basin to basin and day to day, and is not indicated in the conceptual diagram of Fig. 8. This warming above the inversion, which is produced by warm air advection or by horizontal turbulent sensible heat flux convergence from the heated sidewalls that are above the remnants of the nocturnal inversion, increases the heat required to destroy the inversion, since air below the top of the inversion that is being carried up the sidewalls must now be warmed an extra amount to remove it from the underlying inversion.

Interestingly, none of the soundings in the Gruenloch show the development of a CBL at the basin floor, which is in shadow until 0600 CEST (Fig. 5b) and has much weaker sensible heat flux than the Peter Sink through the entire breakup period. The sinking of the elevated remnant of the nocturnal inversion (the ''stable core'') during this same time, however, implies that substantial mass is being carried out from under the stable core in upslope flows that occur on the stable core's margins. These flows are expected to be strongest on the east-facing sidewall where the favorable azimuth and inclination angles produce high sensible heat fluxes during the inversion breakup period. No field studies have yet been performed to observe upslope flows on both sidewalls of a valley during this period. Differences in CBL depth and potential temperature can be expected around the basin periphery because of variations in slope insolation and, consequently, sensible heat flux—a feature anticipated by Brehm (1986) for which no vertical structure observations are yet available. This concept is, however, supported by temperature datalogger observations at the 1.4-m level on the Gruenloch sidewalls (Whiteman et al. 2004a). Temperatures are often 2°–3° warmer on the sunny sidewalls than indicated by con-

current tethered balloon observations over the basin center at the same elevation.

b. Comparative heat deficits

Whiteman et al. (1999b) compared observed near-sunrise heat deficits at 30 sites in nine western U.S. valleys and basins of different size. The deficits were determined from single near-sunrise soundings using the formula $D = 0.5\overline{\rho}c_p h\Delta\theta = 0.5\overline{\rho}c_p\gamma h^2$, where $\overline{\rho}$ is mean air density, h is inversion height, $\Delta\theta$ is the potential temperature difference between the valley floor and the top of the inversion, and γ is the mean potential temperature gradient in the inversion. The heat deficit calculated in this way is the amount of heat that must be added to a sunrise sounding to remove the surface-based inversion and attain a constant potential temperature equal to the potential temperature at the top of the inversion [this simplified formula differs from Eq. (1) by not accounting for the change of volume with height in valleys or basins]. They found that mean potential temperature gradients were typically in the range from 0.020 to 0.035 K m^{-1} and that heat deficits were generally in the range from 2 to 6 MJ m^{-2}. Similar calculations can now be made for the small sinkhole basins. The Peter Sink (9 September) had an extremely strong potential temperature gradient (0.200 K m^{-1}), but a depth of only 120 m, resulting in a heat deficit of 1.45 MJ m^{-2}. The Gruenloch (3 June) had a potential temperature gradient of 0.108 K m^{-1} and a depth of 120 m, resulting in a heat deficit of 0.78 MJ m^{-2}. Thus, these small basins, despite having extreme potential temperature gradients when compared with a range of western U.S. valleys, are seen to have relatively small heat deficits at sunrise that can be overcome earlier by sensible heat flux when the basin is illuminated after sunrise. Further, these computed deficits, because they are calculated without considering the confining topography, somewhat overestimate the actual deficits.

c. Relationship between atmospheric heat budgets and surface energy budgets

Destruction of a basin inversion requires that the air within the basin be warmed to the potential temperature of the air above the inversion. This warming through the bulk of the basin cross section occurs primarily through subsidence warming. The subsidence is a response to the removal of air mass from the base of the inversion by upslope flows above the heated sidewalls. The upslope flows are driven by the convergence of sensible heat flux that warms the shallow boundary layer above the basin floor and sidewalls so that the air in this layer becomes warmer than the air at the same level over the basin center. Heating in the basin cross section is thus driven by sensible heat fluxes on the basin floor and sidewalls. In the following, we will use this conceptual model of inversion destruction and our observations of heat gains in the basin atmospheres to roughly estimate the components of the surface energy budgets over the Peter Sink and Gruenloch basins and to compare the surface partitioning of available energy into latent and sensible heat fluxes in the two basins.

The surface energy budget is given by the equation

$$Q_N + Q_G + Q_H + Q_E = 0, \tag{2}$$

where Q_N is net radiation, Q_G is ground heat flux, Q_H is sensible heat flux, and Q_E is latent heat flux. The sign convention is such that fluxes are positive when directed toward the soil–atmosphere interface, whether from the soil or the atmosphere. This equation applies instantaneously and can be integrated over the time period of inversion breakup to obtain

$$\tilde{Q}_N + \tilde{Q}_G + \tilde{Q}_H + \tilde{Q}_E = 0, \tag{3}$$

where the tildes indicate the time integration.

Net all-wave radiation is approximately sinusoidal and can be represented for a horizontal, nonshaded surface as

$$Q_n = A \sin\left[\frac{\pi}{\tau}(t - t_{\mathrm{SR}})\right] (\mathrm{W\ m^{-2}}), \tag{4}$$

where A is the net radiation at solar noon, τ is the length of the daylight period, t is time, and t_{SR} is the time of astronomical sunrise. By integrating over the time of the inversion breakup period we obtain

$$\tilde{Q}_N = -\frac{\tau A}{\pi}\cos\frac{\pi}{\tau}(t - t_{\mathrm{SR}})\Big|_{t=t_{\mathrm{SR}}}^{t=t_{\mathrm{BU}}} (\mathrm{J\ m^{-2}}), \tag{5}$$

where t_{BU} is the time of inversion breakup. For the Peter Sink, no net radiation data were available on 9 September. The measured values on 12 September (Fig. 6a), however, are a reasonable proxy for 9 September since there was no precipitation in the intervening period and the weather conditions were similar. From Fig. 6a, $A \sim 525$ W m^{-2}; from section 3a, the breakup interval on 9 September was $t_{\mathrm{BU}} - t_{\mathrm{SR}} = 2.6$ h $= 9360$ s; and, from a solar model for the date of 9 September, $\tau = 12.7$ h $= 45\,600$ s. Then $\tilde{Q}_N$, evaluated from (5), is 1.55 MJ m^{-2}. For the Gruenloch on 3 June, $A = 675$ W m^{-2} (Fig. 6b), $t_{\mathrm{BU}} - t_{\mathrm{SR}} = 3$ h $= 10\,800$ s (section 3a), and $\tau = 15.6$ h $= 56\,100$ s (solar model), so that $\tilde{Q}_N = 1.91$ MJ m^{-2}. These values of cumulative net radiation are considered to be representative of the basin drainage areas below 120 m ABF.

The ground heat flux was not measured in either of the basins, but is estimated from measurements made in Colorado's Brush Creek Valley in September 1984. This valley is, like the Peter Sink, at a high elevation and with similar soil characteristics. The average ground heat flux in the 3-h period following sunrise at five widely dispersed and representative sites there was about 20 W m^{-2} (Whiteman et al. 1989b). The sign indicates that, over this period, the net flux of heat is from the ground toward the surface. This flux typically

TABLE 1. Surface energy budget components and extraterrestrial solar radiation ($\tilde{K}_{ext}$) as accumulated over the inversion breakup period (MJ m^{-2}) for the Peter Sink (9 Sep 1999) and Gruenloch basins (3 Jun 2002). Also given is the Bowen ratio β (dimensionless).

Basin	$\tilde{Q}_N$	$\tilde{Q}_G$	$\tilde{Q}_H$	$\tilde{Q}_E$	$\tilde{K}_{ext}$	$\beta = \tilde{Q}_H/\tilde{Q}_E$
Peter Sink	1.55	0.19	−1.10	−0.64	2.84	1.75
Gruenloch	2.14	0.22	−0.45	−1.91	4.13	0.24

reverses near the end of this period as the ground begins its daytime accumulation of energy. Using this value, cumulative ground heat fluxes $\tilde{Q}_G$ for the Peter Sink and Gruenloch basins would be 0.19 and 0.22 MJ m^{-2}.

The cumulative heat gains in the basins up to 120 m ABF and over the time from sunrise to breakup were 1.10 and 0.45 MJ m^{-2}, respectively, for the Peter Sink and Gruenloch (Fig. 7a). Since a basin atmosphere gain represents a surface loss, $\tilde{Q}_H$ is −1.10 and −0.45 MJ m^{-2} for the respective basins. The cumulative sensible heat flux determined from the atmospheric heat budget in the Peter Sink can also be checked against the time-integrated point measurement of sensible heat flux at the basin floor on 12 September (Fig. 6a). The integration to calculate the basinwide cumulative sensible heat flux (say, $\tilde{Q}'_H$) is accomplished using Eq. (5) by replacing $\tilde{Q}_N$ with $\tilde{Q}'_H$ and A with the extrapolated maximum value of the measured sensible heat flux on the basin floor at solar noon (~325 W m^{-2}), and integrating from the time of astronomical sunrise t_{SR} rather than using the delayed local sunrise time at this site caused by shadows cast from the surrounding ridgeline. We obtain $\tilde{Q}'_H = -1.25$ MJ m^{-2}, which compares reasonably well to $\tilde{Q}_H$.

Table 1 shows the resulting estimated energy balances in the two basins from Eq. (3), where the latent heat flux is computed as a residual. The partitioning of surface heat fluxes is quite different in the two basins, with the bulk of the available energy ($\tilde{Q}_N + \tilde{Q}_G$) partitioned into sensible heat flux in the Peter Sink and into latent heat flux in the Gruenloch. The computed Bowen ratios, that is, the ratios of sensible to latent heat fluxes, were 1.75 for the Peter Sink and 0.24 for the Gruenloch. Shown for comparison in the table is the extraterrestrial solar radiation as accumulated over the breakup period. The sensible heat flux is about 39% of the extraterrestrial solar flux in the Peter Sink and 11% of the extraterrestrial flux in the Gruenloch. The rough surface energy balance is credible but, again, the unknown errors in the estimated terms should be emphasized (especially the crude estimate of the Gruenloch soil heat flux) as they will accumulate in the latent heat flux term, which is calculated as a residual.

The fraction of the theoretical incoming (i.e., extraterrestrial) solar radiation at the inversion top that must be converted to sensible heat flux to explain the observed warming in the basins is not constant with time, as shown in Fig. 9. Rather, it decreases with time for both basins, and is initially much higher in the drier Peter Sink basin than in the Gruenloch. Thus, the energy

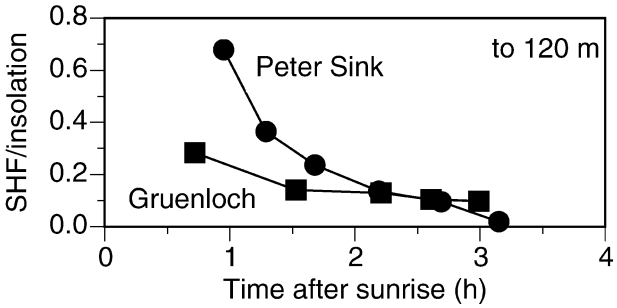

FIG. 9. Ratio of the rate of heat gain in the basin accumulated to a height of 120 m (from Fig. 7b) and the theoretical solar radiation as a function of time after sunrise for 3 Jun 2002 (Gruenloch) and 9 Sep 1999 (Peter Sink).

supplied by net incoming radiation initially goes mostly into sensible heat flux but progressively goes more and more into ground and latent heat fluxes.

d. Comparison of inversion breakup processes in valleys and basins

The patterns of inversion breakup observed in the two sinkhole basins are similar to those observed previously in valleys having substantial valley wind circulations, such as Colorado's Eagle and Yampa valleys (Whiteman 1982) and Germany's Loisach valley (Müller and Whiteman 1988). This suggests that the essential features of the inversion destruction pattern are independent of the existence or nonexistence of valley winds. An early hypothesis offered to explain the sinking of the top of a valley inversion after sunrise was the draining of the nocturnal valley cold air pool down the valley's axis after sunrise (Ayer 1961). The sinking of the top of the inversions in the two sinkholes cannot be explained in this way, since the basins are confined volumes in which no along-valley wind systems (i.e., drainage flows) were present. The sinkhole data also provide additional evidence to refute the hypothesis (e.g., Davidson and Rao 1963) that the sinking of the inversion top is caused by turbulent erosion at the top of the cold pool. Inversions in the sinkholes were destroyed after sunrise when winds above the cold pools were generally less than 1.5 m s^{-1} (Fig. 4).

The pattern-2 inversion breakup in the Gruenloch can be compared with pattern-2 breakups that have been previously observed in the Gore and Yampa valleys of Colorado (Whiteman 1982) and with the partial data from the snow-covered Gruenloch collected by Sauberer and Dirmhirn (1954) that suggested a similar breakup pattern. In the Gore and Yampa valleys, pattern-2 inversion destructions were observed when snow cover was present and the rate of input of sensible heat flux to the valley atmosphere was small. The Gruenloch observations show that pattern-2 inversions also occur in small basins and, in agreement with the valley observations, that they occur when sensible heat fluxes are

small—in this case because most of the available energy is partitioned into latent heat flux rather than sensible heat flux. When the rate of input of sensible heat flux is rapid, a pattern-3 inversion destruction is observed in both valleys and basins.

6. Conclusions

The breakup of nocturnal temperature inversions has been investigated in two, high-altitude, limestone sinkholes or basins in the Rocky Mountains and Alps of about 2 km^2 size. The two basins, the Peter Sink and Gruenloch basins, respectively, were located in very different climate settings. The Peter Sink had dry soil and low atmospheric humidity, while the Gruenloch had moist soil and high humidity. At sunrise, surface-based inversions were 120 m deep in both basins, but the potential temperature increase between the basin floor and the inversion top was 24 K in the Peter Sink and only 13 K in the Gruenloch.

The basin inversions were destroyed 2.6 and 3.0 h after sunrise, respectively. This is a shorter time than the 3.5–5 h reported for deeper valleys. The rapid breakups were attributed to the relatively small heat deficits in the shallow basins at sunrise; these deficits can be overcome earlier by sensible heat flux once the basin is illuminated after sunrise. The time required to destroy the inversions was nearly the same in the two basins, despite the big difference in inversion strengths. Weaker inversions develop overnight in the Gruenloch because the rate of loss of sensible heat from the basin atmosphere is reduced in the moist climate setting. The rate of release of sensible heat flux after sunrise is also diminished, as much of the available incoming energy is used to support evaporation. The weaker inversion and the lower rate of input of sensible heat flux in the Gruenloch balance the stronger inversion and higher rate of sensible heat flux in the drier Peter Sink, resulting in similar inversion breakup times.

The rate of sensible heat flux input to the Peter Sink atmosphere was estimated from observations of the changes in atmospheric heat storage in the two basins. When integrated over the inversion breakup periods, the heat flux input to the Peter Sink atmosphere was 2.44 times greater than that to the Gruenloch atmosphere. A rough estimate of the components of the surface energy budget in the two sinkholes, obtained from measurements and some simple assumptions, showed that the two basins had quite different Bowen ratios, with the predominant portion of the available energy going to support evaporation in the Gruenloch and sensible heat flux in the Peter Sink.

We have developed a conceptual model of basin inversion breakup that emphasizes the cross-basin inhomogeneities and temporal evolution of boundary layer structure that occur when sunlight moves progressively down the east-facing sidewall as the sun rises above the ridgeline east of the basin. The temperature structure in the remnants of the nocturnal inversion remains stable and approximately horizontally stratified as a deeper and deeper convective boundary layer develops over the heated sidewall and gradually extends deeper into the basin. A cross-basin flow develops to support the movement of air up the heated sidewall. The inversion top sinks as mass is removed from the valley by upslope flows in the developing convective boundary layer.

The patterns of inversion breakup found in the closed and relatively stagnant basins are similar to those observed previously in well-drained valleys, adding to previous evidence that valley wind systems cannot be responsible for the breakup patterns and, specifically, for inversion top descent. The inversion destruction pattern in the Gruenloch basin has been seen previously only in snow-covered valleys and appears to occur only when the rate of input of sensible heat flux is weak.

Acknowledgments. We thank the participants of the Peter Sink experiment. Doctor John Horel helped to organize the Peter Sink experiments, Dr. Jerry Allwine (Pacific Northwest National Laboratory, PNNL) provided preexperiment tethersonde calibrations, essential in-field support, and postexperiment analysis advice, and Mr. Burt Tanner and Mr. Ed Swiatek (Campbell Scientific, Inc.) provided processed data from their net radiometer and sonic anemometer. We thank students and staff at the University of Utah for essential field support and for their assistance in operating the tethersonde. Assistance came from Mark Beaty, Linda Cheng, Carol Ciliberti, Justin Cox, Lacey Holland, Galdino Mota, Steve Nesbitt, Mike Splitt, and Jebb Stewart. The Logan office of the Wasatch–Cache National Forest is thanked for providing a special-use permit.

We also thank the other organizers and participants of the 2001–02 Gruenloch experiments, including Dr. M. Hantel (University of Vienna), K. Baumann-Stanzer (Central Institute for Meteorology and Geodynamics), and the many students at the University of Vienna who assisted with the field observations; Mr. P. Kupelwieser is thanked for providing access to the Gruenloch experimental area.

This research was supported by the U.S. Department of Energy (DOE) under the auspices of the Atmospheric Sciences Program of the Office of Biological and Environmental Research. The research was conducted at PNNL, which is operated for the U.S. DOE by Battelle Memorial Institute. One of the authors (CBC) was supported by a Graduate Research Environmental Fellowship funded by DOE's Global Change Education Program. Two of the authors (SE and BP) thank the University of Vienna, the state of Lower Austria, DOE, and PNNL for fellowships served at PNNL in 2002 and 2003.

REFERENCES

Ayer, H. S., 1961: On the dissipation of drainage wind systems in valleys in the morning hours. *J. Meteor.*, **18,** 560–563.

Bader, D. C., and T. B. McKee, 1983: Dynamical model simulation of the morning boundary layer development in deep mountain valleys. *J. Climate Appl. Meteor.,* **22,** 341–351.

——, and ——, 1985: Effects of shear, stability and valley characteristics on the destruction of temperature inversions. *J. Climate Appl. Meteor.,* **24,** 822–832.

——, and C. D. Whiteman, 1989: Numerical simulation of cross-valley plume dispersion during the morning transition period. *J. Appl. Meteor.,* **28,** 652–664.

Banta, R. M., 1984: Daytime boundary-layer evolution over mountainous terrain. Part I: Observations of the dry circulations. *Mon. Wea. Rev.,* **112,** 340–356.

——, and W. R. Cotton, 1981: An analysis of the structure of local wind systems in a broad mountain basin. *J. Appl. Meteor.,* **20,** 1255–1266.

Brehm, M., 1986: Experimentelle und numerische Untersuchungen der Hangwindschicht und ihrer Rolle bei der Erwärmung von Tälern (Experimental and numerical investigations of the slope wind layer and its role in the warming of valleys). Ph.D. dissertation, Universität München, Meteorologisches Institut, 169 pp.

Bretschko, G., and P. Adamicka, 1998: Meteorology and the Biological Station Lunz (Austria). *Wetter Leben,* **50,** 89–101.

Clements, C. B., C. D. Whiteman, and J. D. Horel, 2003: Cold air pool structure and evolution in a mountain basin: Peter Sinks, Utah. *J. Appl. Meteor.,* **42,** 752–768.

Colette, A., F. K. Chow, and R. L. Street, 2003: A numerical study of inversion-layer breakup and the effects of topographic shading in idealized valleys. *J. Appl. Meteor.,* **42,** 1255–1272.

Davidson, B., and P. K. Rao, 1963: Experimental studies of the valley-plain wind. *Int. J. Air Water Pollut.,* **7,** 907–923.

Fast, J., S. Zhong, and C. D. Whiteman, 1996: Boundary layer evolution within a canyonland basin. Part II: Numerical simulations of nocturnal flows and heat budgets. *J. Appl. Meteor.,* **35,** 2162–2178.

Geiger, R., 1965: *The Climate near the Ground.* Harvard University Press, 482 pp.

Hennemuth, B., 1986: Thermal asymmetry and cross-valley circulation in a small Alpine valley. *Bound.-Layer Meteor.,* **36,** 371–394.

Iijima, Y., and M. Shinoda, 2000: Seasonal changes in the cold-air pool formation in a subalpine hollow, central Japan. *Int. J. Climatol.,* **20,** 1471–1483.

Kondo, J., T. Kuwagata, and S. Haginoya, 1989: Heat budget analysis of nocturnal cooling and daytime heating in a basin. *J. Atmos. Sci.,* **46,** 2917–2933.

Litschauer, D., 1962: Untersuchung der Entwicklung von Kaltluftseen in Dolinen- und Beckenlagen (Investigation of the development of cool air pools in sinkholes and basins). Ph.D. dissertation, University of Vienna, 129 pp.

Magono, C., C. Nakamura, and Y. Yoshida, 1982: Nocturnal cooling of the Moshiri Basin, Hokkaido in midwinter. *J. Meteor. Soc. Japan,* **60,** 1106–1116.

Maki, M., and T. Harimaya, 1988: The effect of advection and accumulation of downslope cold air on nocturnal cooling in basins. *J. Meteor. Soc. Japan,* **66,** 581–597.

——, T. Harimaya, and K. Kikuchi, 1986: Heat budget studies on nocturnal cooling in a basin. *J. Meteor. Soc. Japan,* **64,** 727–740.

Marty, C., and R. Philipona, 2001: Surface radiation and cloud forcing over the Alps. *IRS 2000: Current Problems in Atmospheric Radiation,* W. L. Smith and Y. M. Timofeyev, Eds., A. Deepak, 688–691.

Mori, M., and T. Kobayashi, 1996: Dynamic interaction between observed nocturnal drainage winds and a cold air lake. *J. Meteor. Soc. Japan,* **74,** 247–258.

Müller, H., and C. D. Whiteman, 1988: Breakup of a nocturnal temperature inversion in the Dischma Valley during DISKUS. *J. Appl. Meteor.,* **27,** 188–194.

Pope, D., and C. Brough, 1996: *Utah's Weather and Climate.* Publishers Press, 245 pp.

Sakiyama, S. K., 1990: Drainage flow characteristics and inversion breakup in two Alberta mountain valleys. *J. Appl. Meteor.,* **29,** 1015–1030.

Sauberer, F., and I. Dirmhirn, 1954: Über die Entstehung der extremen Temperaturminima in der Doline Gstettner-Alm (On the occurrence of extreme temperature minimums in the Gstettner-Alm Doline). *Arch. Meteor. Geophys. Bioklimatol.,* **5B,** 307–326.

——, and ——, 1956: Weitere Untersuchungen über die kaltluftansammlungen in der Doline Gstettner-Alm bei Lunz in Niederösterreich (Further investigations of the cold air buildup in the Gstettner-Alm doline near Lunz in lower Austria). *Wetter Leben,* **8,** 187–196.

——, and ——, 1958: Das Strahlungsklima. *Klimatographie von Österreich,* F. Steinhauser, O. Eckel, and F. Lauscher, Eds., Springer, 13–102.

Segal, M., and J. Davis, 1992: The impact of deep cumulus reflection on the ground-level global irradiance. *J. Appl. Meteor.,* **31,** 217–222.

Smith, R., and Coauthors, 1997: Local and remote effects of mountains on weather: Research needs and opportunities. *Bull. Amer. Meteor. Soc.,* **78,** 877–892.

Steinacker, R., M. Dorninger, S. Eisenbach, A. M. Holzer, B. Pospichal, C. D. Whiteman, and E. Mursch-Radlgruber, 2002: A sinkhole field experiment in the Eastern Alps. Preprints, *10th Conf. on Mountain Meteorology,* Park City, UT, Amer. Meteor. Soc., 91–92.

Urfer-Henneberger, C., 1970: Neure Beobachtungen über die Entwicklung des Schönwetterwindsystems in einem V-förmigen Alpental (Dischmatal bei Davos) [New observations of the development of a clear weather wind system in a v-shaped mountain valley (Dischma Valley near Davos)]. *Arch. Meteor. Geophys. Bioklimatol.,* **18B,** 21–42.

Whiteman, C. D., 1982: Breakup of temperature inversions in deep mountain valleys: Part I. Observations. *J. Appl. Meteor.,* **21,** 270–289.

——, 1989: Morning transition tracer experiments in a deep narrow valley. *J. Appl. Meteor.,* **28,** 626–635.

——, and T. B. McKee, 1982: Breakup of temperature inversions in deep mountain valleys: Part II. Thermodynamic model. *J. Appl. Meteor.,* **21,** 290–302.

——, and K. J. Allwine, 1986: Extraterrestrial solar radiation on inclined surfaces. *Environ. Software,* **1,** 164–169.

——, ——, L. J. Fritschen, M. M. Orgill, and J. R. Simpson, 1989a: Deep valley radiation and surface energy budget microclimates. Part I: Radiation. *J. Appl. Meteor.,* **28,** 414–426.

——, ——, ——, ——, and ——, 1989b: Deep valley radiation and surface energy budget microclimates. Part II: Energy budget. *J. Appl. Meteor.,* **28,** 427–437.

——, T. B. McKee, and J. C. Doran, 1996: Boundary layer evolution within a canyonland basin. Part I: Mass, heat, and moisture budgets from observations. *J. Appl. Meteor.,* **35,** 2145–2161.

——, X. Bian, and S. Zhong, 1999a: Wintertime evolution of the temperature inversion in the Colorado Plateau basin. *J. Appl. Meteor.,* **38,** 1103–1117.

——, S. Zhong, and X. Bian, 1999b: Wintertime boundary layer structure in the Grand Canyon. *J. Appl. Meteor.,* **38,** 1084–1102.

——, ——, W. J. Shaw, J. M. Hubbe, X. Bian, and J. Mittelstadt, 2001: Cold pools in the Columbia basin. *Wea. Forecasting,* **16,** 432–447.

——, S. Eisenbach, B. Pospichal, and R. Steinacker, 2004a: Comparison of vertical soundings and sidewall air temperature measurements in a small Alpine basin. *J. Appl. Meteor.,* in press.

——, T. Haiden, B. Pospichal, S. Eisenbach, and R. Steinacker, 2004b: Minimum temperatures, diurnal temperature ranges, and temperature inversions in limestone sinkholes of different sizes, and shape. *J. Appl. Meteor.,* **43,** 1224–1236.

Yoshino, M. M., 1984: Thermal belt and cold air drainage on the mountain slope and cold air lake in the basin at quiet, clear night. *GeoJournal,* **8,** 235–250.

Zhong, S., C. D. Whiteman, X. Bian, W. J. Shaw, and J. M. Hubbe, 2001: Meteorological processes affecting the evolution of a wintertime cold air pool in the Columbia basin. *Mon. Wea. Rev.,* **129,** 2600–2613.